Instability analysis and simulation of water infiltration into an unsaturated elasto-viscoplastic material

AUTHOR(S):

Garcia, E.; Oka, F.; Kimoto, S.

Instability analysis and simulation of water infiltration into an unsaturated elasto-viscoplastic material

E. Garcia[1], F. Oka* and S. Kimoto

Department of Civil and Earth Resources Engineering
Kyoto University, Kyotodaigaku-katsura 4, Nishikyo-ku, Kyoto, 615-8540, Japan

*Corresponding author:
Kyoto University, Kyotodaigaku-katsura 4, Nishikyo-ku, Kyoto, 615-8540, Japan
Tel: +81-75-383-3191; fax: +81+75-383-3193
Email Address: oka.fusao.2s@kyoto-u.ac.jp

[1]On leave from Department of Civil Engineering (Lecturer), University of Antioquia - Colombia

ABSTRACT

A linear instability analysis was performed in order to investigate which variables have a significant effect on the onset of the instability of an unsaturated viscoplastic material subjected to water infiltration. It was found that the onset of the growing instability of the material system mainly depends on the specific moisture capacity, the suction, and the hardening parameter. Then, in order to simulate the water infiltration process of a one-dimensional unsaturated soil column, a multiphase coupled elasto-viscoplastic finite element analysis was performed based on the theory of porous media. The results of the numerical simulations are discussed with respect to the effect of the specific moisture capacity and the initial suction on the development of volumetric strain. We found that rapid transitions from unsaturated to saturated states and higher levels of initial suction lead to the contractive behavior of the material and instability. The instability detected by the numerical results is consistent with the theoretical results obtained through the linear instability analysis.

KEY WORDS: Instability; unsaturated soil; elasto-viscoplastic; infiltration; numerical analysis

1. INTRODUCTION

It has been well recognized that the behavior of unsaturated soil subjected to water infiltration plays an important role in Geomechanics. This is because the failure of natural slopes, embankments, and artificial soil structures is most often due to water infiltration. The failure of soil structures can be triggered by a wetting process from an unsaturated stage resulting from an increase in moisture content and a decrease in suction. Jennings and Burland (1962) conducted a series of consolidation tests and showed that partly saturated soil upon wetting undergoes additional settlement or “collapses”; this phenomenon is commonly referred to as collapse behavior. To study this behavior in unsaturated soil, several constitutive models have been developed (e.g., Alonso et al., 1990; Cui and Delage, 1996; Oka et al., 2006; Sheng et al., 2003; Thomas and He, 1998; Wheeler and Karube, 1996; Wheeler and Sivakumar, 1995). Simultaneously, unsaturated seepage-deformation coupled methods have been developed in order to solve practical geotechnical problems for unsaturated soil (e.g., Alonso et al., 2003; Cho and Lee, 2001; Ehlers et al., 2004; Kato et al., 2009; Oka et al., 2009).

The instability of saturated porous media has been widely studied by many researchers (e.g., Ehlers and Volk, 1998; Higo et al., 2005, 2006; Loret and Prévost, 1991; Oka et al., 1994, 1995; Rice, 1975; Schrefler et al., 1995) from both experimental and analytical points of view. However, studies on the instability of unsaturated porous materials have not been completed. Many experimental and numerical researches have been conducted on the deformation behavior of unsaturated soil (e.g., Alonso et al., 2003; Cunningham et al., 2003; Feng, 2007; Khalili et al., 2004; Kimoto et al., 2007; Oka et al., 2010). Nevertheless, the deformation of unsaturated soil is still a subject of research. And theoretical analyses, such as instability analyses, have not yet been performed. Recently, Buscarnera and Nova (2009a, 2009b) addressed the general problem of soil instability for partially saturated geomaterials with particular reference to the controllability of oedometric and triaxial conditions. They showed that the onset of instability can be identified by several hydro-mechanical tests, in which wetting processes may explain the main cause of soil instability. In addition, Garcia et al. (2010) studied the effect of hydraulic parameters on the transient vertical infiltration problem and their effect on the

deformation behavior of elasto-viscoplastic unsaturated soil. Among the hydraulic parameters studied, it was found that the generation of pore water pressure and volumetric strain is significantly controlled by the material parameters that describe the soil water characteristic curve.

The main objective of the present paper is to study the effect of parameters and state variables on the unstable behavior of unsaturated materials when they are subjected to a wetting process, e.g., rainfall and flooding. Then, before conducting the numerical analysis, the material parameters and the conditions that contribute to the growth rate of the fluctuation are examined via a linear instability analysis. From this analysis, it is found that the onset of the instability of the material system depends on the specific moisture capacity (slope of the soil water characteristic curve), the suction, and the hardening parameter.

The multiphase coupled elasto-viscoplastic finite element analysis formulation proposed by Oka et al. (2006) is used to describe the water infiltration into a one-dimensional column and the transition of the porous material from an unsaturated state to a saturated state. The numerical analyses presented here are based on the fundamental concept of the theory of porous media, (e.g., Atkin and Craine, 1976; Biot, 1962; Bowen, 1976). The materials are assumed to be composed of solid, water, and air which are thought to be continuously distributed throughout space at a macroscopic level. An elasto-viscoplastic constitutive model is adopted for the soil skeleton (Kimoto and Oka, 2005). The skeleton stress, which is determined from the difference between the total stress and the average pore fluid pressure, is used for the stress variable in the governing equations. In addition, the constitutive parameters are functions of the matric suction, by which the shrinkage or the expansion of the overconsolidation boundary surface and the static yield surface can be described (Oka et al., 2006).

The paper is organized as follows: In *Section 2*, a seepage-deformation coupled method is described within the framework of a macroscopic continuum approach through the use of the theory of porous media. In *Section 3*, a linear instability analysis is presented in order to investigate the effect of material parameters on the onset of the instability of the governing equations using a simplified one-dimensional viscoplastic model. In the analytical formulation, the material is assumed to be a triphasic continuum

consisting of a soil skeleton, pore water, and pore air. In *Section 4*, numerical simulations of the one-dimensional water infiltration problem are presented to discuss the effect of the specific moisture capacity and the initial suction on the development of volumetric strain. For the numerical simulation, an updated Lagrangian method with the objective Jaumman rate of Cauchy stress is adopted (Kimoto et al., 2004; Oka et al., 2006). It is shown that the instability obtained by the numerical analyses is consistent with the theoretical results obtained by the linear instability analysis.

2. MULTIPHASE COUPLED ELASTO-VISCOPLASTIC FORMULATION

2.1 Governing equations

Unsaturated material is assumed to be composed of three phases, namely, solid (S), water (W), and air (G), which are continuously distributed throughout space. Total volume V and volume of the voids V^V are obtained from the sum of the partial volumes of the constituents, namely,

$$V = V^S + V^W + V^G \tag{1}$$

$$V^V = V^W + V^G \tag{2}$$

Volume fraction n^α ($\alpha = S$, W, and G) is defined as the ratio of the specific volume element with respect to the total volume, namely,

$$n^\alpha = \frac{V^\alpha}{V} \tag{3}$$

$$n^S + n^W + n^G = 1 \tag{4}$$

The porosity, n, is written as

$$n = \frac{V^V}{V} = \frac{V - V^S}{V} = 1 - n^S \tag{5}$$

In addition, water saturation s smaller than 1 indicates that the medium is unsaturated. s is defined as

$$s = \frac{V^W}{V^V} = \frac{V^W}{V^W + V^G} = \frac{n^W}{n} \tag{6}$$

2.1.1 Skeleton stress

Terzaghi (1943) defined the effective stress for water-saturated soil. In the case of unsaturated soil, however, the effective stress needs to be redefined in order to include a third phase, namely, the air phase. This phase is considered to be compressible. In the present formulation, skeleton stress tensor σ'_{ij} is defined and then used for the stress variable in the constitutive relation for the soil skeleton (Kimoto et al., 2010, 2007).

The partial stresses of the water and air phases express as

$$\sigma_{ij}^{W} = -n^{W} P^{W} \delta_{ij} \tag{7}$$

$$\sigma_{ij}^{G} = -n^{G} P^{G} \delta_{ij} \tag{8}$$

where P^W and P^G are the pore water pressure and the pore air pressure, respectively.

The partial stress tensor for the solid phase can be expressed by an analogy with the water-saturated phase as

$$\sigma_{ij}^{S} = \sigma'_{ij} - n^{S} P^{F} \delta_{ij} \tag{9}$$

where P^F is the average pore pressure. Total stress tensor σ_{ij} is obtained from the sum of the partial stresses, namely,

$$\sigma_{ij} = \sigma_{ij}^{S} + \sigma_{ij}^{W} + \sigma_{ij}^{G} \qquad \text{S=Solid, W=Water, G=Air.} \tag{10}$$

Substituting Equations (7) to (9) into Equation (10), and considering Equations (4) to (6), we have

$$\sigma'_{ij} = \sigma_{ij} + P^{F} \delta_{ij} \tag{11}$$

where σ'_{ij} is the skeleton stress, which is used as the basic stress variable in the model for unsaturated soil. In Equation (11), the average pore pressure is given by

$$P^{F} = sP^{W} + (1-s)P^{G} \tag{12}$$

2.1.2 Conservation of mass

The conservation of mass for the soil, the water, and the air phases is given by the following equations:

$$\frac{D^{\alpha}}{Dt}\left(n^{\alpha}\rho_{\alpha}\right) + n^{\alpha}\rho_{\alpha} v_{i,i}^{\alpha} = 0 \qquad \alpha = S, W, G \tag{13}$$

in which ρ_α and v_i^α are the material density and the velocity of each phase, respectively. $\frac{D^\alpha}{Dt}$ denotes the material time derivative following particles of phase α.

Supposing that the soil skeleton and water are incompressible, namely, $\dot{\rho}_S = 0$ and $\dot{\rho}_W = 0$, the conservation laws of Equation (13) yield

$$\dot{n}^S \rho_S + n^S \rho_S v_{i,i}^S = 0 \tag{14}$$

$$\dot{n}^W \rho_W + n^W \rho_W v_{i,i}^W = 0 \tag{15}$$

$$\dot{n}^G \rho_G + n^G \dot{\rho}_G + n^G \rho_G v_{i,i}^G = 0 \tag{16}$$

where the superimposed dot denotes the material time derivative following particles of each phase, respectively.

Considering Equations (5) and (6), Equations (14) to (16) provide

$$-\dot{n}\rho_S + (1-n)\rho_S v_{i,i}^S = 0 \tag{17}$$

$$\dot{n}\, s\, \rho_W + n\, \dot{s}\, \rho_W + n\, s\, \rho_W v_{i,i}^W = 0 \tag{18}$$

$$\dot{n}(1-s)\rho_G - n\dot{s}\rho_G + n(1-s)\dot{\rho}_G + n(1-s)\rho_G v_{i,i}^G = 0 \tag{19}$$

The apparent velocity or flux vector V_i^β of water and air, with respect to the solid phase, is defined as

$$V_i^\beta = n^\beta \left(v_i^\beta - v_i^S\right) \qquad \beta = W, G \tag{20}$$

Multiplying Equation (17) by $s(\rho_W/\rho_S)$, adding Equation (18), and considering Equation (20), the continuity equation for the water phase can be obtained as

$$s v_{i,i}^S + n\dot{s} = -V_{i,i}^W \tag{21}$$

Similarly, multiplying Equation (17) by $(1-s)\rho_G/\rho_S$, adding Equation (19), and considering Equation (20), the continuity equation for the gas phase can be obtained as

$$(1-s)v_{i,i}^S - n\dot{s} + n(1-s)\frac{\dot{\rho}_G}{\rho_G} = -V_{i,i}^G \tag{22}$$

To describe the changes in air density, the equation for ideal gas is used, i.e.,

$$\rho^G = \frac{MP^G}{R\theta} \tag{23}$$

$$\dot{\rho}^G = \frac{M}{R}\left(\frac{\dot{P}^G}{\theta} - \frac{P^G\dot{\theta}}{\theta^2}\right) \tag{24}$$

in which M is the molecular weight of the gas, R is the gas constant, and θ is the temperature.

2.1.3 Conservation of momentum

The momentum balance equations for the three phases are given by

$$n^{\alpha}\rho_{\alpha}\dot{v}_i^{\alpha} = \sigma_{ji,j}^{\alpha} + \rho_{\alpha}n^{\alpha}\overline{F}_i + \sum_{\gamma} D^{\alpha\gamma}\left(v_i^{\alpha} - v_i^{\gamma}\right) \qquad \alpha,\gamma = S,W,G \tag{25}$$

in which $\overline{F}_i$ is the gravitational force per unit mass and $D^{\alpha\gamma}$ ($D^{\alpha\gamma}$=$D^{\gamma\alpha}$) are the parameters which describe the interaction between phases α and γ, which is defined as

$$D^{WS} = -\frac{\left(n^W\right)^2\rho_W g}{k^W}, \qquad D^{GS} = -\frac{\left(n^G\right)^2\rho_G g}{k^G} \tag{26}$$

in which k^W and k^G are the permeability coefficients for the water phase and the air phase, respectively.

Disregarding the acceleration and the interaction between air and water, the momentum balance equations for the three phases are obtained as

$$\sigma'_{ji,j} - \left(n^S P^F\right)_{,i} + \rho_S n^S \overline{F}_i + D^{SW}\left(v_i^S - v_i^W\right) + D^{SG}\left(v_i^S - v_i^G\right) = 0 \tag{27}$$

$$-\left(n^W P^W\right)_{,i} + \rho_W n^W \overline{F}_i + D^{WS}\left(v_i^W - v_i^S\right) = 0 \tag{28}$$

$$-\left(n^G P^G\right)_{,i} + \rho_G n^G \overline{F}_i + D^{GS}\left(v_i^G - v_i^S\right) = 0 \tag{29}$$

Supposing that the distribution of porosity is sufficiently smooth and using Equation (26), Darcy's laws for the water and the air phases are obtained from Equations (28) and (29), respectively, as

$$V_i^W = n^W\left(v_i^W - v_i^S\right) = -\frac{k^W}{\rho_W g}\left(P_{,i}^W - \rho_W \overline{F}_i\right) \tag{30}$$

$$V_i^G = n^G\left(v_i^G - v_i^S\right) = -\frac{k^G}{\rho_G g}\left(P_{,i}^G - \rho_G \overline{F}_i\right) \tag{31}$$

The sum of Equations (27) to (29) leads to the equilibrium equation for the whole mixture

$$\sigma_{ji,j} + \rho\overline{F}_i = 0 \tag{32}$$

where ρ is the density of the mixture.

2.2 Constitutive equations for the soil

2.2.1 Soil water characteristic curve (SWCC)

The relation between suction $P^C=P^G-P^W$ and effective saturation s_{re} is given by the equation proposed by van Genuchten (1980) as

$$s_{re} = \left\{1 + \left(\alpha P^C\right)^{n'}\right\}^{-m} \tag{33}$$

$$s_{re} = \frac{s - s_{\min}}{s_{\max} - s_{\min}} \tag{34}$$

in which α, n', and m are material parameters, and the relation $m = 1\text{-}1/n'$ is assumed. s_{max} and s_{min} are the maximum and the minimum limiting values of saturation, respectively. The relationship between m and n' leads to an S-shaped type of soil water characteristic curve.

The effects of the degree of saturation on permeability for water and air are assumed as

$$k^W = k_s^W s^a \left\{1 - \left(1 - s^{\frac{1}{m}}\right)^{n'}\right\}, \quad k^G = k_s^G (1-s)^b \left\{1 - \left(s^{\frac{1}{m}}\right)^{n'}\right\} \tag{35}$$

where a and b are the material parameters, and m and n' are the parameters in the van Genuchten equation. k_s^W is the coefficient of permeability for water under saturated conditions and k_s^G is the coefficient of permeability for air under fully dry conditions.

From Equations (33) and (34), it is seen that the *SWCC* is mainly controlled by parameters α and n'. Parameter α is related to the air-entry value condition, which is the suction value at which the maximum saturation starts to decrease due to air entering the soil. Parameter n' is related to the pore size distribution of the soil. Figure 1 illustrates the effect of parameter α on the air-entry value and the *SWCC* for constant parameter n'. This figure shows that when parameter α increases, the air-entry value decreases. Soils with relatively high air-entry values, e.g., clays, are characterized by smaller values for α. Similarly, Figure 2 illustrates the effect of parameter n' on the *SWCC* for constant parameter α. In this figure, it is seen that the soil water characteristic curve becomes steeper for the larger values of n'; soils with steeper curves, e.g., sands, are represented by larger parameters n'. Additional details concerning the physical meaning and the effects of these constitutive parameters on the hydraulic behavior of unsaturated soils can be found in Lu and Likos (2004) and Pinder and Gray (2008).

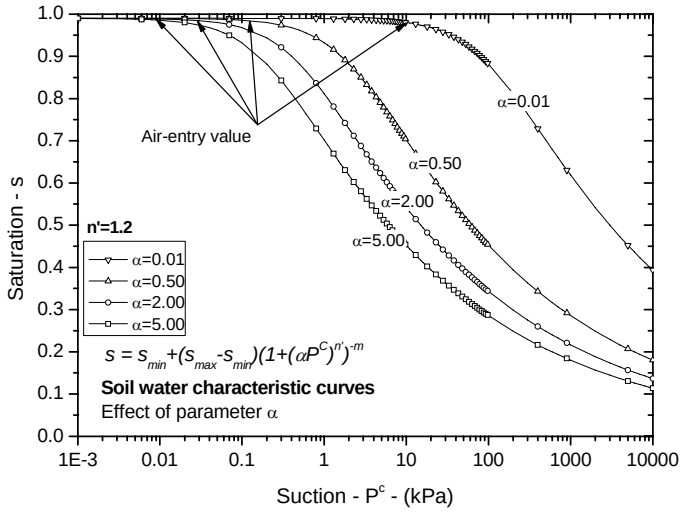

Figure 1: Effect of parameter α on the soil water characteristic curve

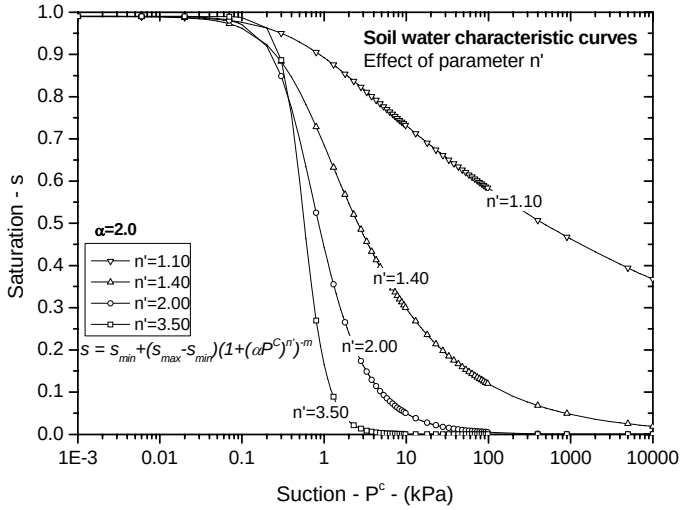

Figure 2: Effect of parameter n' on the soil water characteristic curve

2.2.2 Elasto-viscoplastic model for unsaturated soil

An elasto-viscoplastic model, based on the overstress-type of viscoplastic theory with soil structure degradation for saturated soil (Kimoto and Oka, 2005), has been extended to

unsaturated soils using the skeleton stress and the suction effect in the constitutive model (Oka et al., 2006).

It is assumed that total strain rate tensor $\dot{\varepsilon}_{ij}$ consists of elastic strain rate tensor $\dot{\varepsilon}^e_{ij}$ and viscoplastic strain rate tensor $\dot{\varepsilon}^{vp}_{ij}$ as

$$\dot{\varepsilon}_{ij} = \dot{\varepsilon}^e_{ij} + \dot{\varepsilon}^{vp}_{ij} \tag{36}$$

The elastic strain rate tensor is given by a generalized Hooke type of law, i.e.,

$$\dot{\varepsilon}^e_{ij} = \frac{1}{2G}\dot{S}_{ij} + \frac{\kappa}{3(1+e_0)}\frac{\dot{\sigma}'_m}{\sigma'_m}\delta_{ij} \tag{37}$$

where S_{ij} is the deviatoric stress tensor, σ'_m is the mean skeleton stress, G is the elastic shear coefficient, e_0 is the void ratio, κ is the swelling index, and the superimposed dot denotes the material time derivative following particles of solid phase.

In this model, it is assumed that there is an overconsolidation (OC) boundary surface that delineates the normally consolidated (NC) region, $f_b \geq 0$, and the overconsolidated region (OC), $f_b < 0$. Overconsolidation boundary surface f_b and static yield function f_y are defined as follows:

$$f_b = \overline{\eta}^*_{(0)} + M^*_m \ln(\sigma'_m / \sigma'_{mb}) = 0 \tag{38}$$

$$f_y = \overline{\eta}^*_{(0)} + \tilde{M}^* \ln(\sigma'_m / \sigma'^{(s)}_{my}) = 0 \tag{39}$$

$$\overline{\eta}^*_{(0)} = \left\{(\eta^*_{ij} - \eta^*_{ij(0)})(\eta^*_{ij} - \eta^*_{ij(0)})\right\}^{\frac{1}{2}}, \qquad \eta^*_{ij} = \frac{S_{ij}}{\sigma'_m} \tag{40}$$

where M^*_m is the value of $\eta^* = \sqrt{\eta^*_{ij}\eta^*_{ij}}$ when the volumetric strain increment changes from contraction to dilation, which is equal to ratio M^*_f at the critical state, σ'_{mb} is the hardening parameter, and $\sigma'^{(s)}_{my}$ is the static hardening parameter. The effect of the unsaturated soil is incorporated for both boundaries as

$$\sigma'_{mb} = \sigma'_{ma} \exp\left(\frac{1+e_0}{\lambda-\kappa}\varepsilon^{vp}_{kk}\right)\left[1 + S_I \exp\left\{-S_d\left(\frac{P^c_i}{P^c} - 1\right)\right\}\right] \tag{41}$$

$$\sigma'^{(s)}_{my} = \frac{\sigma'^{(s)}_{myi}}{\sigma'_{mai}}\sigma'_{ma} \exp\left(\frac{1+e_0}{\lambda-\kappa}\varepsilon^{vp}_{kk}\right)\left[1 + S_I \exp\left\{-S_d\left(\frac{P^c_i}{P^c} - 1\right)\right\}\right] = \frac{\sigma'^{(s)}_{myi}}{\sigma'_{mai}}\sigma'_{mb} \tag{42}$$

where ε^{vp}_{kk} is the viscoplastic volumetric strain, λ is the compression index, and e_0 is the initial void ratio. $P^C{}_i$ is the initial suction value, P^C is the present suction value, and S_I is

the material parameter that denotes the strength ratio to the saturated soil when suction is P^C_i. S_d is the parameter which controls the rate of increase or decrease in strength. σ'_{ma} is a strain-softening parameter used to describe the degradation of the material caused by structural changes, namely,

$$\sigma'_{ma} = \sigma'_{maf} + (\sigma'_{mai} - \sigma'_{maf})\exp(-\beta z) \tag{43}$$

$$z = \int_0^t \dot{z}dt\,, \quad \dot{z} = \sqrt{\dot{\varepsilon}^{vp}_{ij}\dot{\varepsilon}^{vp}_{ij}} \tag{44}$$

in which σ'_{mai} and σ'_{maf} are the initial and the final values of σ'_{ma}, respectively, β is a material parameter which controls the rate of structural changes, and z is the accumulation of the second invariant of viscoplastic strain rate $\dot{\varepsilon}^{vp}_{ij}$.

Details of the constitutive model with soil structure degradation are given by Kimoto and Oka (2005).

The viscoplastic potential surface is described as

$$f_p = \overline{\eta}^*_{(0)} + \tilde{M}^* \ln(\sigma'_m / \sigma'_{mp}) = 0 \tag{45}$$

where $\tilde{M}^*$ is assumed to be constant in the NC region and to vary with the current stress in the OC region as

$$\tilde{M}^* = \begin{cases} M^*_m & : \text{NC region} \\ -\dfrac{\sqrt{\eta^*_{ij}\eta^*_{ij}}}{\ln(\sigma'_m/\sigma'_{mc})} & : \text{OC region} \end{cases} \tag{46}$$

where M^*_m is the value of $\sqrt{\eta^*_{ij}\eta^*_{ij}}/\sigma'_m$ at the critical state, and σ'_{mc} denotes the mean skeleton stress at the intersection of the OC boundary surface and the σ'_m axis as

$$\sigma'_{mc} = \sigma'_{mb}\exp\frac{\sqrt{\eta^*_{ij(0)}\eta^*_{ij(0)}}}{M^*_m} \tag{47}$$

Finally, the viscoplastic strain rate tensor is given by the following equation when $f_y>0$, which is based on Perzyna's type of viscoplastic theory (Oka et al., 2004) as

$$\dot{\varepsilon}^{vp}_{ij} = C_{ijkl}\sigma'_m \exp\left\{m'\left(\overline{\eta}^*_{(0)} + \tilde{M}^* \ln\frac{\sigma'_m}{\sigma'_{mb}}\right)\right\}\frac{\partial f_p}{\partial \sigma'_{kl}} \tag{48}$$

$$C_{ijkl} = D\delta_{ij}\delta_{kl} + E(\delta_{ik}\delta_{jl} + \delta_{il}\delta_{jk}),\ C_1 = 2E,\ C_2 = 3D + 2E$$

in which C_1 and C_2 are the viscoplastic parameters for the deviatoric and the volumetric components, respectively.

3. ONE-DIMENSIONAL INSTABILITY ANALYSIS OF AN UNSATURATED VISCOPLASTIC MATERIAL

Jennings and Burland (1962) conducted a series of consolidation tests on unsaturated soils and showed that upon wetting, the soil samples collapsed; this phenomenon is commonly referred to as collapse behavior, i.e., instability problem. In recent years, many researches have been oriented to study the behavior of unsaturated soils (e.g., Alonso et al., 2003; Buscarnera and Nova, 2009b; Cunningham et al., 2003; Ehlers et al., 2004; Khalili et al., 2004; Kimoto et al., 2007; Oka et al., 2010).

In spite of the above-mentioned valuable works, the effects of the constitutive parameters on the deformation of an unsaturated material have not yet been fully investigated. Hence, the deformation behavior of unsaturated soils has to be studied with both numerical simulations and an instability analysis. In the present section, a linear instability analysis is conducted on an unsaturated material in a viscoplastic state in order to examine which constitutive parameters and conditions lead to the onset of a growing instability during a wetting process.

Due to the high nonlinearity of the hydraulic and the constitutive equations involved in the unsaturated coupled seepage-deformation analysis method, only simplified one-dimensional analytical solutions for the infiltration problem can be obtained for elastic materials (e.g., Wu and Zhang, 2009). Therefore, the linear instability analysis will be applied to a one-dimensional viscoplastic unsaturated material based on the multiphase coupled seepage-deformation framework presented in *Section 2*. The results by the instability analysis obtained here will be discussed with the numerical simulation results in *Section 4*.

3.1 Governing equations

3.1.1 Stress variables

Following *Section 2*, one-dimensional stress variables are defined in the following. From Equations (7) to (11), the one-dimensional total and partial stresses can be rewritten as

$$\sigma^W = -n^W P^W \tag{49}$$

$$\sigma^G = -n^G P^G \tag{50}$$

$$\sigma^S = \sigma' - n^S P^F \tag{51}$$

$$\sigma = \sigma^S + \sigma^W + \sigma^G \tag{52}$$

$$\sigma' = \sigma + P^F \tag{53}$$

The average fluid pressure acting on the solid phase is given by Equation (12) as

$$P^F = sP^W + (1-s)P^G \tag{54}$$

where s is the saturation.

3.1.2 Constitutive equation

A simplified viscoplastic constitutive model is used in this analysis. The stress-strain relation can be written as

$$\sigma' = H\varepsilon + \mu\dot{\varepsilon} \tag{55}$$

where ε is the strain, $\dot{\varepsilon}$ is the strain rate, H is the strain hardening-softening parameter, which is a function of suction P^C, and μ is the viscoplastic parameter.

Suction P^C is included in the constitutive model and is defined by

$$P^C = P^G - P^W \tag{56}$$

3.1.3 Equation of equilibrium

The one-dimensional equilibrium equation can be written from Equation (32) as follows:

$$\frac{\partial \sigma}{\partial x} + \rho\overline{F} = \frac{\partial \sigma'}{\partial x} - \frac{\partial P^F}{\partial x} + \rho\overline{F} = 0 \tag{57}$$

3.1.4 Continuity equations

In the one-dimensional analysis, the continuity equations for the water and the air phases, can be written from Equations (21) and (22), respectively,

$$s\dot{\varepsilon} + n\dot{s} = -\frac{\partial V^W}{\partial x} \tag{58}$$

$$(1-s)\dot{\varepsilon} - n\dot{s} + n(1-s)\frac{\dot{\rho}_G}{\rho_G} = -\frac{\partial V^G}{\partial x} \tag{59}$$

3.1.5 Darcy's law

Darcy's laws for the flow of water and air can be obtained from Equations (30) and (31), namely,

$$V^W = -\frac{k^W}{\gamma_W}\left\{\frac{\partial P^W}{\partial x} - \rho_W \overline{F}\right\} \tag{60}$$

$$V^G = -\frac{k^G}{\gamma_G}\left\{\frac{\partial P^G}{\partial x} - \rho_G \overline{F}\right\} \tag{61}$$

3.2 Perturbed governing equations

Next, we consider the equilibrium equation, continuity equations, and constitutive equations in the perturbed configuration. The perturbations of pore water pressure P^W, pore air pressure P^G, and strain ε in a one-dimensional form are assumed to be of the periodic form, as

$$\begin{bmatrix} \tilde{P}^W \\ \tilde{P}^G \\ \tilde{\varepsilon} \end{bmatrix} = \begin{bmatrix} P^{W*} \\ P^{G*} \\ \varepsilon^* \end{bmatrix} \exp(iqx + \omega t) \tag{62}$$

where q is the wave number ($=2\pi/l$, l: wave length), ω is the growth rate of the fluctuation, and superscript * indicates the amplitude of each variable.

The perturbation of the equilibrium equation, Equation (57), is given by

$$\frac{\partial \tilde{\sigma}}{\partial x} = \frac{\partial \tilde{\sigma}'}{\partial x} - \frac{\partial \tilde{P}^F}{\partial x} = 0 \tag{63}$$

where the perturbed variables are indicated by a tilde. $\tilde{\sigma}'$ can be written from Equation (55) as

$$\tilde{\sigma}' = \tilde{H}\varepsilon + H\tilde{\varepsilon} + \mu\dot{\tilde{\varepsilon}} \tag{64}$$

Since strain hardening -softening parameter H is a function of the suction; the perturbation of H is given as

$$\tilde{H} = \frac{\partial H}{\partial P^C}\tilde{P}^C = A\tilde{P}^C \tag{65}$$

where A ($=\partial H/\partial P^C$) indicates the slope of the H-P^C curve.

Using Equations (62), (64~65), and considering that $\dot{\tilde{\varepsilon}} = \omega\tilde{\varepsilon}$, we have a spatial differentiation of the perturbed skeleton stress as

$$\frac{\partial\tilde{\sigma}'}{\partial x} = \left(A\varepsilon P^{G*} - A\varepsilon P^{W*} + H\varepsilon^* + \mu\omega\varepsilon^*\right)iq\exp(iqx+\omega t) \tag{66}$$

Similarly, $\tilde{P}^F$ can be written by means of Equation (54) as

$$\tilde{P}^F = \tilde{s}P^W + s\tilde{P}^W + (1-s)\tilde{P}^G - \tilde{s}P^G \tag{67}$$

In Equation (67), the degree of saturation, s, is a function of suction through a constitutive equation such as van Genuchten Equations (33~34). Then, the perturbed degree of saturation is given as

$$\tilde{s} = \frac{\partial s}{\partial P^C}\tilde{P}^C = B\tilde{P}^C \tag{68}$$

where B ($=\partial s/\partial P^C$) indicates the slope of the s-P^C curve. B is called the specific moisture capacity.

Using Equations (62), (67) and (68), we have a gradient of the perturbed average pore pressure as

$$\frac{\partial\tilde{P}^F}{\partial x} = \left(\left(-BP^W + s + BP^G\right)P^{W*} + \left(BP^W + 1 - s - BP^G\right)P^{G*}\right)iq\exp(iqx+\omega t) \tag{69}$$

By substituting Equations (66) and (69) into Equation (63) and rearranging the terms, we obtain

$$-\left(A\varepsilon + BP^C + s\right)P^{W*} + \left(A\varepsilon + BP^C + s - 1\right)P^{G*} + \left(H + \mu\omega\right)\varepsilon^* = 0 \tag{70}$$

The perturbation of the continuity equation for the water phase (58) is given by

$$\tilde{s}\,\dot{\varepsilon} + s\dot{\tilde{\varepsilon}} + n\dot{\tilde{s}} = -\frac{\partial\tilde{V}^W}{\partial x} \tag{71}$$

where the perturbed rate of the degree of saturation and the perturbed spatial differentiation of the Darcy Equation for the water (60) can be written, respectively, as

$$\tilde{\dot{s}} = \omega B \tilde{P}^C \tag{72}$$

$$\frac{\partial \tilde{V}^W}{\partial x} = \frac{\partial}{\partial x}\left[-\frac{k^W}{\gamma_W}\left\{ \frac{\partial \tilde{P}^W}{\partial x} \right\} \right] = -\frac{k^W}{\gamma_W}\frac{\partial^2 \tilde{P}^W}{\partial x^2} \tag{73}$$

By substituting Equations (62), (68), (72), and (73) into Equation (71) and rearranging the terms, we obtain

$$-\left(B\dot{\varepsilon} + n\omega B - q^2 \frac{k^W}{\gamma_W} \right) P^{W*} + \left(B\dot{\varepsilon} + n\omega B \right) P^{G*} + s\omega\varepsilon^* = 0 \tag{74}$$

For the sake of simplicity, it is considered that the time rate of the air density is equal to zero; as a result, the perturbation of the continuity equation for the air phase (59) is given by

$$(1-s)\tilde{\dot{\varepsilon}} - \tilde{\dot{s}}\,\dot{\varepsilon} - n\tilde{\dot{s}} = -\frac{\partial \tilde{V}^G}{\partial x} \tag{75}$$

The perturbed spatial differentiation of the Darcy Equation for the air (61) can be written as

$$\frac{\partial \tilde{V}^G}{\partial x} = \frac{\partial}{\partial x}\left[-\frac{k^G}{\gamma_G}\left\{ \frac{\partial \tilde{P}^G}{\partial x} \right\} \right] = -\frac{k^G}{\gamma_G}\frac{\partial^2 \tilde{P}^G}{\partial x^2} \tag{76}$$

Upon substitution of Equations (62), (68), (72), and (76) into Equation (75) and rearranging the terms, we obtain

$$\left(B\dot{\varepsilon} + n\omega B \right) P^{W*} - \left(B\dot{\varepsilon} + n\omega B - q^2 \frac{k^G}{\gamma_G} \right) P^{G*} + (1-s)\omega\varepsilon^* = 0 \tag{77}$$

Finally, we can rewrite the perturbed equilibrium and continuity equations for water and air, Equations (70), (74), and (77), in matrix form as

$$\begin{bmatrix} -\left(A\varepsilon + BP^C + s\right) & \left(A\varepsilon + BP^C + s - 1\right) & \left(H + \mu\omega\right) \\ -\left(B\dot{\varepsilon} + Bn\omega - q^2 \frac{k^W}{\gamma_W} \right) & \left(B\dot{\varepsilon} + Bn\omega\right) & \left(s\omega\right) \\ \left(B\dot{\varepsilon} + Bn\omega\right) & -\left(B\dot{\varepsilon} + Bn\omega - q^2 \frac{k^G}{\gamma_G} \right) & (1-s)\omega \end{bmatrix} \begin{Bmatrix} P^{W*} \\ P^{G*} \\ \varepsilon^* \end{Bmatrix} = [A]\{y\} = \{0\} \tag{78}$$

For nonzero values of P^{W*}, P^{G*}, and ε^*, the determinant of matrix [A] has to be equal to zero. From det[A]=0, we have a polynomial function of ω as

$$\omega^2 + \alpha_1 \omega + \alpha_2 = 0 \tag{79}$$

in which

$$\alpha_1 = \frac{1}{-Bn\left\{\gamma_G \gamma_W + \left(\gamma_W k^G + \gamma_G k^W\right) q^2 \mu\right\}} \left[q^2 \left\{ \gamma_W k^G s^2 + \left(A\varepsilon + BP^C\right)\left(\gamma_W k^G s - \gamma_G k^W (1-s)\right) + \gamma_G k^W \left(s^2 - 2s + 1\right) \right.\right. \\ \left.\left. - B\left(\gamma_W k^G + \gamma_G k^W\right)\left(nH + \dot{\varepsilon}\mu\right) + k^W k^G \mu q^2 \right\} - B\dot{\varepsilon}\gamma_W \gamma_G \right] \tag{80}$$

$$\alpha_2 = \frac{1}{-Bn\left\{\gamma_G \gamma_W + \left(\gamma_W k^G + \gamma_G k^W\right) q^2 \mu\right\}} \left\{ - B\dot{\varepsilon}\left(\gamma_W k^G + \gamma_G k^W\right) + k^G k^W q^2 \right\} q^2 H \tag{81}$$

In the following, we discuss the onset of the instability of the material system. If the growth rate of perturbation ω, which is the root of Equation (79), has a negative real part, the material system is stable. On the contrary, if ω has a positive real part, the material system is unstable. In order to estimate whether the real part of ω is negative or positive, we adopt the Routh-Hurwitz criteria. The roots of Equation (79) have negative real parts when the coefficients of the characteristic polynomial satisfy

$$\alpha_1 > 0, \quad \alpha_2 > 0 \tag{82}$$

The first factor in Equations (80) and (81) is positive. Thus, it is sufficient to consider the sign of the variables in the second factor for the analysis, namely,

$$\alpha_1^* = \left[q^2 \left\{ \gamma_W k^G s^2 + \left(A\varepsilon + BP^C\right)\left(\gamma_W k^G s - \gamma_G k^W (1-s)\right) + \gamma_G k^W \left(s^2 - 2s + 1\right) \right.\right. \\ \left.\left. - B\left(\gamma_W k^G + \gamma_G k^W\right)\left(nH + \dot{\varepsilon}\mu\right) + k^W k^G \mu q^2 \right\} - B\dot{\varepsilon}\gamma_W \gamma_G \right] > 0 \tag{83}$$

$$\alpha_2^* = \left\{ - B\dot{\varepsilon}\left(\gamma_W k^G + \gamma_G k^W\right) + k^G k^W q^2 \right\} q^2 H > 0 \tag{84}$$

Note that in Equations (83) and (84), the terms q, s, n, μ, k^W, k^G, γ_W, and γ_G are positive, as well as the term $\left(s^2 - 2s + 1\right)$, because s<1. Considering that the unit weight of the air is much smaller than the unit weight of the water ($\gamma_G / \gamma_W \approx 0.001$), we can reasonably assume that the term $\left(\gamma_W k^G s - \gamma_G k^W (1-s)\right)$ is always positive for the typical permeabilities of the soils. This condition is satisfied by the water and air permeabilities used in the simulations in *Section 4*.

Additionally, we analyze the sign of the terms A, B, strain ε, and strain rate $\dot{\varepsilon}$, in Equations (83) and (84), as follows:

1) Parameter H decreases when the suction decreases; consequently, the slope of the H-P^C curve is positive, i.e., $A>0$.

2) Saturation increases when the suction decreases; therefore, the slope of the s-P^C curve is negative, i.e., $B<0$.

3) Strain ε is positive in extension and negative in contraction, and strain rate $\dot{\varepsilon}$ can be positive or negative.

Now, let us consider the stability of the model when parameter H is positive, i.e., viscoplastic hardening; from Equations (83) and (84) it is possible that α^*_1 and α^*_2 can be negative in the following cases:

1) Large B

B is negative, hence when B is large, term BP^C in α^*_1 is more negative. Moreover, if strain rate $\dot{\varepsilon}$ is negative, terms $-B\dot{\varepsilon}$ included in α^*_1 and α^*_2 become negative; namely, the possibility of instability is more likely.

2) Large Suction

If P^C increases, the term BP^C becomes more negative; consequently, α^*_1 can be negative more easily.

3) Large A ($=\partial H/\partial P^C$) *and negative strain* $\varepsilon<0$

In this case, when A becomes larger while the strain is negative, $\varepsilon<0$ (compression or contraction), term $A\varepsilon$ is more negative. As a result, it is possible that α^*_1 becomes more negative.

4) Large Viscoplastic parameter μ *and negative strain rate* $\dot{\varepsilon} < 0$

If the strain rate is negative, namely, contractive, term $\dot{\varepsilon}\mu$ in α^*_1 becomes negative. In addition, if the viscoplastic parameter μ is large, term α^*_1 becomes more negative.

Similarly, for the case in which strain hardening-softening parameter H is negative, i.e., viscoplastic softening, α^*_1 and α^*_2 can also be negative. Then, similar conditions exist for the onset of the instability of the material system.

Until now, the conditions for the onset of the instability of an unsaturated material system have been shown by means of an analytical analysis using a viscoplastic model and the linear instability analysis. From the analysis, it can be said that in both hardening

and softening ranges, the onset of the instability of a material in a viscoplastic state mainly depends on terms BP^C and $A\varepsilon$, as well as strain rate $\dot{\varepsilon}$. In *Section 4*, the results of various simulations of the one-dimensional infiltration problem will be presented in order to study the material instability by the model proposed in *Section 2*. The numerical analyses are based on the effect of the variation in parameters α and n', which controls the soil water characteristic curve as well as specific moisture capacity B (slope of the *SWCC*) and initial suction $P^C{}_i$. The effect of these parameters on the generation of volumetric strain ε is presented.

4. NUMERICAL ANALYSIS BY AN ELASTO-VISCOPLASTIC MODEL

4.1 Simulation of the one-dimensional infiltration problem

In the numerical simulation a finite element formulation based on the finite deformation theory has been used in which strain rate tensor $\dot{\varepsilon}_{ij}$ in *Section 2* is replaced by the deformation rate tensor D_{ij} for the constitutive model (Kimoto et al. 2004; Oka et al. 2006). In addition, an updated Lagrangian method with the objective Jaumann rate of Cauchy stress tensor $\hat{T}'_{ij}$ is adopted in this formulation. The rate type of conservation for the momentum, by the material derivative of the equilibrium equations in the current configuration, is used for the updated Lagrangian formulation of the boundary value problem (Fung and Tong, 2001; Nemat-Nasser, 2004).

Weak forms of the continuity equations for water and air and the rate type of conservation of momentum are discretized in space and solved by the finite element method. In the finite element formulation, the independent variables are the pore water pressure, the pore air pressure, and the nodal velocity. An eight-node quadrilateral element with a reduced Gaussian integration is used for the displacement, and four nodes are used for the pore water pressure and the pore air pressure. The backward finite difference method is used for the time discretization.

The finite element mesh and the boundary conditions for the simulations are shown in Figure 3. A homogeneous soil column with a depth of 1 m is employed in the simulations. An undrained boundary for water is assigned at the bottom and on the lateral sides of the column. Air flux is allowed both at the bottom and at the top of the column. The top of the column is subjected to a pore water pressure equal to 4.9 kPa. The simulations of the infiltration process start from an unsaturated condition where initial suction $P^C{}_i$ is the same along the column. At t=0, water starts to infiltrate due to the pore water pressure applied at the top until a hydrostatic condition is attained in the column. Different values for the van Genuchten parameters (Section 2.2.1); parameter α, from α=0.1 to α=10 (1/kPa), and parameter n', from n'=1.01 to n'=9.0, as well as two different levels of initial suction, $P^C{}_i$=25.5 (Case 1) and 100 kPa (Case 2), were considered to study the instability of the unsaturated material system. The material parameters required by the constitutive model introduced here are listed in Table 1. Figure 4 shows an example of the results for a time history of the pore water pressure distribution obtained by the simulations. This figure shows a transition of the soil from an initial unsaturated state ($P^C{}_i$=25.5 kPa) to a saturated state corresponding to the hydrostatic condition.

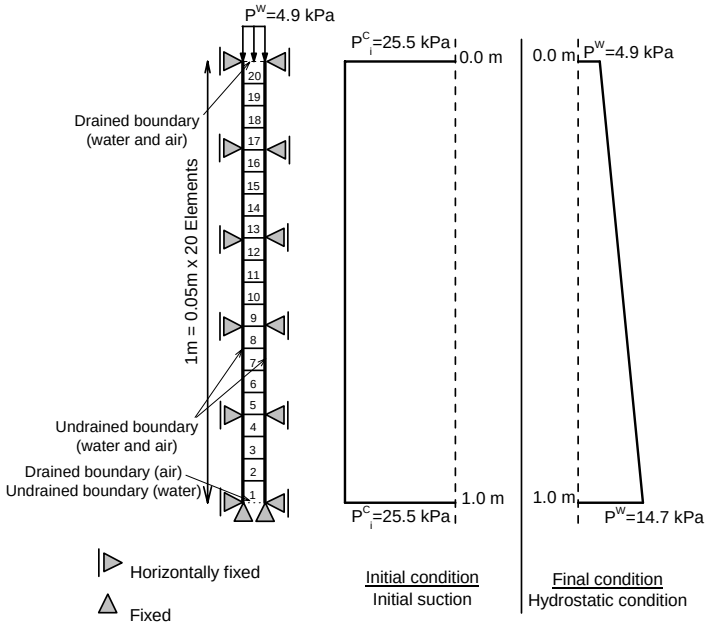

Figure 3: Finite element mesh and boundary conditions

Table 1: Material parameters for the simulations

Viscoplastic parameter	m'	*23.0*
Viscoplastic parameter (1/s)	C_1	1.0×10^{-8}
Viscoplastic parameter (1/s)	C_2	1.0×10^{-8}
Stress ratio at critical state	M^*_m	*0.947*
Parameter of tangent line rigid method	θ	*0.5*
Coefficient of water permeability at s=1.0 (m/s)	k^W_s	1.83×10^{-5}
Coefficient of air permeability at s=0.0 (m/s)	K^G_s	1.00×10^{-3}
Compression index	λ	*0.136*
Swelling index	κ	*0.0175*
Initial shear elastic modulus (kPa)	G_0	*4000*
Initial void ratio	e_0	*0.5983*
Structural parameter	β	*0.0*
Suction parameter	S_I	*0.2*
Suction parameter	S_d	*0.25*
Minimum saturation	s_{min}	*0.0*
Maximum saturation	s_{max}	*0.99*
Parameter of coefficient of water permeability	a	*3.0*
Parameter of coefficient of air permeability	b	*2.3*

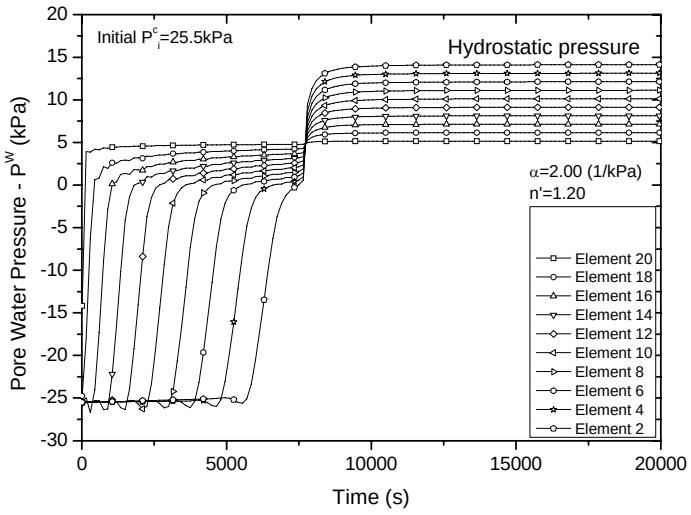

Figure 4: Time history of pore water pressure (α=2.00 1/kPa, n'=1.20, P^C_i=25.5 kPa)

In the following sections, the discussion intends to show a trend in the deformation behavior of unsaturated soil as well as the consistency between the numerical results and the theoretical results obtained in Section 3. It is worth noting that the onset of the

instability of the unsaturated viscoplastic material subjected to a wetting process can be interpreted as the sudden increase in contractive volumetric deformation during the numerical analysis. This contractive behavior (collapse behavior) can be attained if the soil presents an open potentially unstable unsaturated structure which can also be attained when relatively high suction or applied stress exists (Barden et al., 1973; Lloret and Alonso, 1980; Wheeler and Sivakumar, 1995). Finally, in order to show the potentially stable and unstable regions of the one-dimensional infiltration problem, the results of the simulation will be plotted in the α-n' space, where the effect of the initial suction is also included.

4.2 Significance of the values for BP^C and $A\varepsilon$ on the onset of the instability of the unsaturated material

In *Section 3,* it was shown that the onset of the instability of the material system depends mainly on values BP^C and $A\varepsilon$ and strain rate $\dot{\varepsilon}$. Among these terms, $\dot{\varepsilon}$ depends on the deformation pattern of the soil during the infiltration process, and its effect on the onset of the instability of the unsaturated material is addressed later (*Section 4.5*). To estimate which of the other two terms has a more significant effect on the onset of the instability of the material, the values corresponding to $A\varepsilon$ and BP^C, included in Equation (83), are investigated during the infiltration process. Firstly, the strength degradation due to the decrease in suction is shown schematically in Figure 5, and the relation between the strain-hardening parameter and the suction is given by Equation (41). From this equation, A is obtained as

$$A = \frac{\partial \sigma'_{mb}}{\partial P^C} = \sigma'_{ma} \exp\left(\frac{1+e_0}{\lambda-\kappa}\varepsilon_{kk}^{vp}\right)\left[S_1 \exp\left(-S_d\left(\frac{P_i^C}{P^C}-1\right)\right)\right]\left[S_d \frac{P_i^C}{P^{C2}}\right] \quad (85)$$

In the same manner, the slope of the *SWCC* can be obtained from Equations (33) and (34) as

$$B = \frac{\partial s}{\partial P^C} = -\alpha m n' \left(s_{\max} - s_{\min}\right)\left(\alpha P^C\right)^{n'-1}\left\{1+\left(\alpha P^C\right)^{n'}\right\}^{-m-1} \quad (86)$$

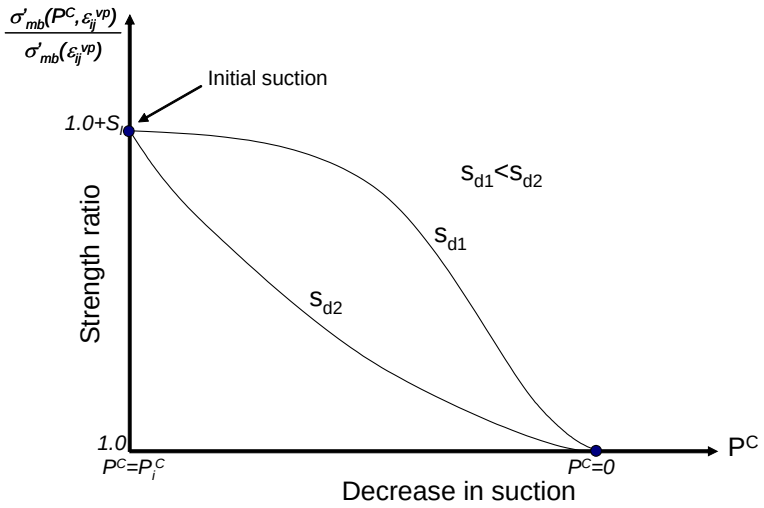

Figure 5: Strength degradation due to the decrease in suction

In the analysis of the one-dimensional soil column, strain ε in Equation (83) corresponds to both the axial strain and the volumetric strain ($\varepsilon=\varepsilon_x=\varepsilon_v$). Using Equations (85) and (86), values $A\varepsilon_v$ and BP^C can be calculated. Figures 6 and 7 show comparisons of the time histories of values $A\varepsilon_v$ and BP^C, respectively, for different parameters α, namely, α =0.5. 1.0, 2.0, and 3.0 (1/kPa), with the same parameter n'=1.4 and the same initial suction $P^C{}_i$=100 kPa during the infiltration process. Figure 6 shows negative values for $A\varepsilon_v$ because the calculated volumetric strain is negative $\varepsilon_v<0$ (contraction). Similarly, Figures 8 and 9 show comparisons of the time histories of values $A\varepsilon_v$ and BP^C, respectively, for different parameters n', namely, n'=1.1, 1.2, 1.3, 1.4, 1.5, and 1.6, with the same parameter α=1.0 (1/kPa) and the same initial suction $P^C{}_i$=100 kPa. In Figure 8 positive values for $A\varepsilon_v$ indicate positive volumetric strain $\varepsilon_v>0$ (expansion or extension) and negative values for $A\varepsilon_v$ when $\varepsilon_v<0$ (contraction). Figures 6 and 8 show that negative values for $A\varepsilon$ increase when parameters α and n' increase. However, they are smaller than the negative values obtained for BP^C (see Figures 7 and 9). This suggests that the effect of term BP^C on the onset of the instability of the material is more significant. Accordingly, it can be said that the onset of the stability of the unsaturated elasto-viscoplastic material in an infiltration process depends mainly on specific moisture capacity B and suction P^C.

In the following section, the effect of B and P^C on the development of volumetric strain will be studied.

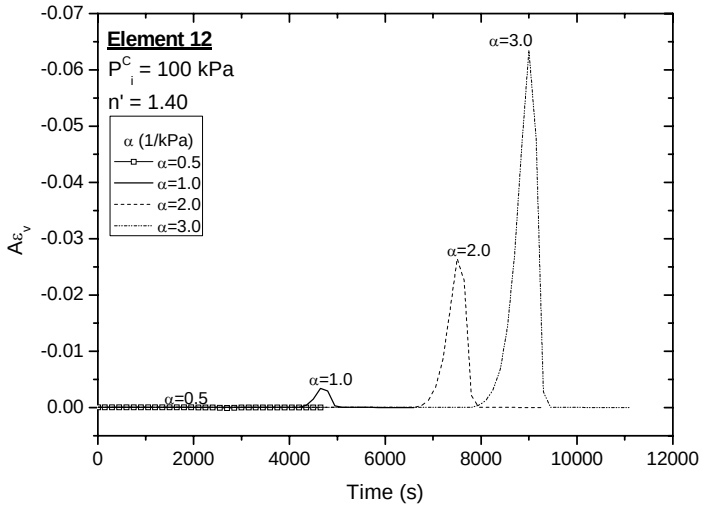

Figure 6: Time history of value $A\varepsilon_v$ for different parameters α

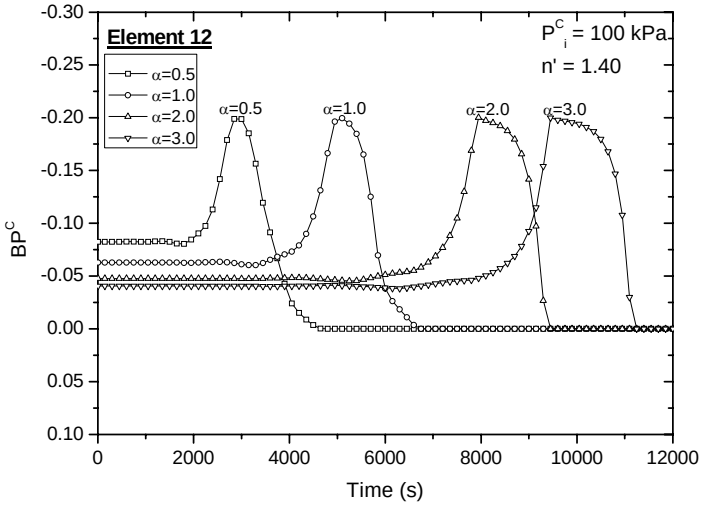

Figure 7: Time history of value BP^C for different parameters α

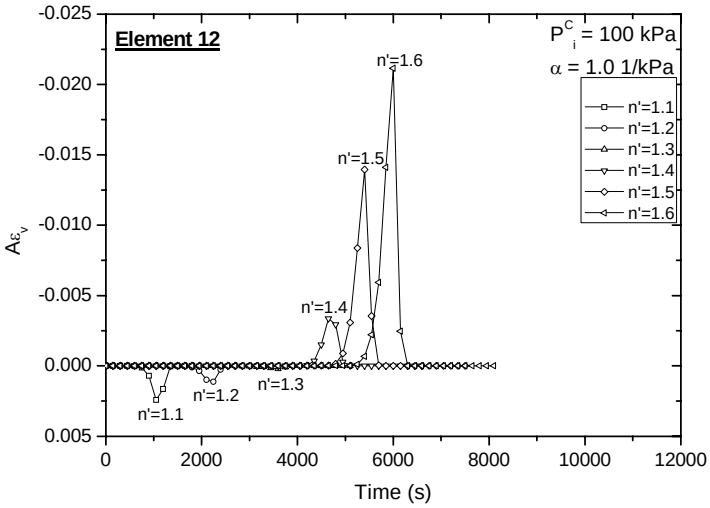

Figure 8: Time history of value $A\varepsilon_v$ for different parameters n'

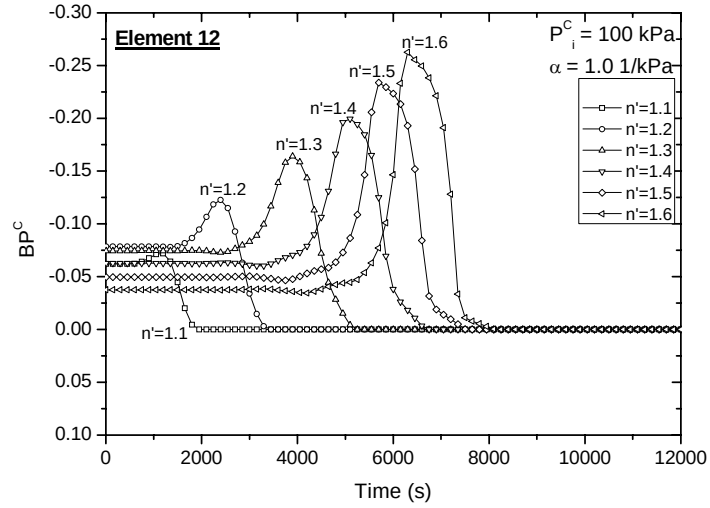

Figure 9: Time history of value BP^C for different parameters n'

4.3 Effect of specific moisture capacity *B* on the onset of the instability of the unsaturated material

According to the instability analysis presented in *Section 3* and using a multiphase viscoplastic model, the material system can be unstable if the magnitude of *B,* which corresponds to the slope of the soil water characteristic curve ($B=\partial s/\partial P^C$), increases. In

the formulation presented in *Section 2*, B plays an important role in the continuity equations for both water and air phases. In addition to the *SWCC*, B (in Equation 86) is also mainly controlled by parameters α and n'.

In the following, a discussion on the effect of parameters α and n' and suction P^C on the development of the volumetric strain is presented.

4.3.1 Effect of parameter α on specific moisture capacity B and volumetric strain ε_v

Figure 10 shows the variation in B due to the changes in suction for different α values when n'=1.4. This figure shows that the value of B is smaller for the higher values of suction. However, when the suction starts to decrease, the value of B increases until it reaches a maximum peak that depends on the α value; the larger the parameter α, the greater the peak for B. After this peak, the value of B starts to decrease toward zero for P^C=0.

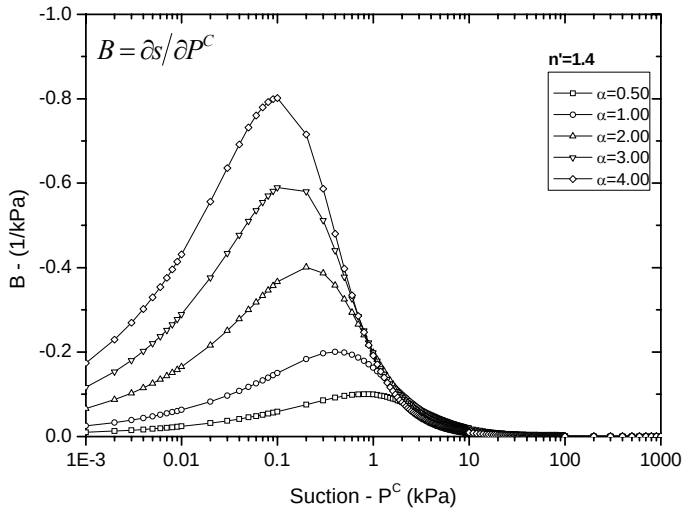

Figure 10: The influence of parameter α on the variation in B ($\partial s/\partial P^C$)

Five different values are considered for parameter α to show its effect on the water infiltration process and the development of volumetric strain (α=0.5, 1.0, 2.0, 3.0, and 4.0 1/kPa). Figure 11 shows the influence of parameter α on the development of volumetric strain ε_v for Element 12 (in Figure 3) when the material is subjected to infiltration from

an initial suction, P^C_i=25.5 kPa (Case 1). From this figure, it is seen that the volumetric strain changes from expansive to contractive when parameter α increases. A similar trend is observed for Case 2 (Figure 12), in which the initial suction is P^C_i= 100 kPa. The increase in parameter α means an increase in B and an increase in the contractive behavior of the soil, and therefore, the potential for instability. These numerical results are consistent with the theoretical results obtained in the linear instability analysis in *Section 3*, where it was shown that the onset of instability increases when B and the contractive strain increase. This means that soils with greater parameters α are potentially more unstable than soils with smaller parameters α.

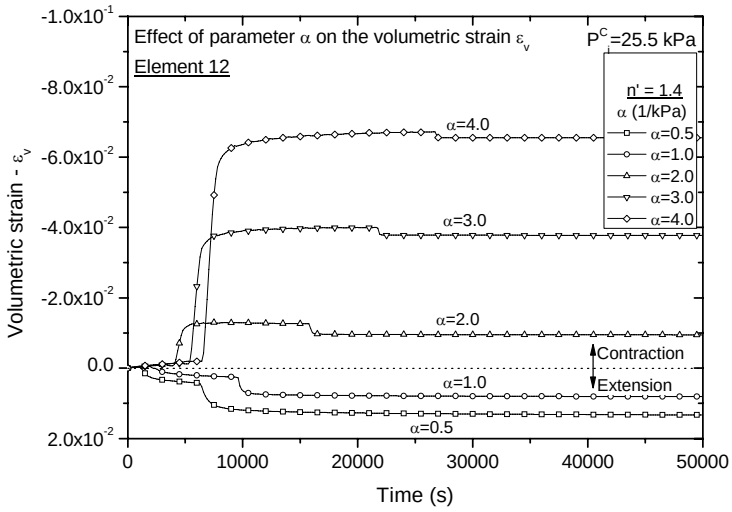

Figure 11: The influence of parameter α on the development of volumetric strain (P^C_i=25.5 kPa)

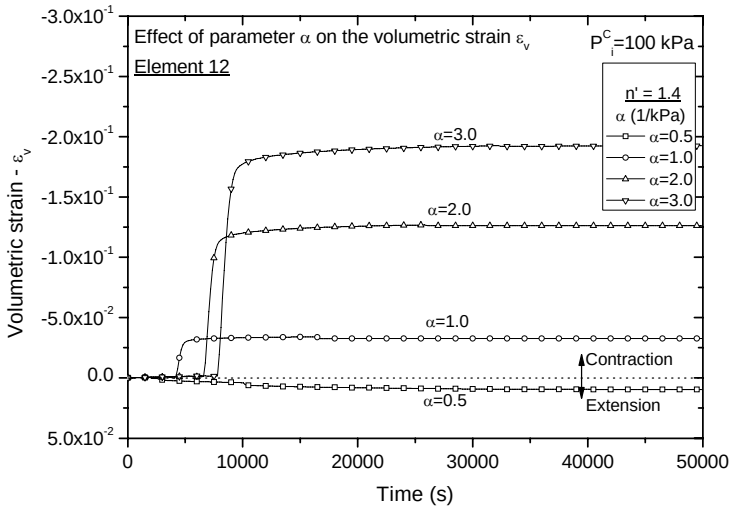

Figure 12: The influence of parameter α on the development of volumetric strain (P^C_i=100 kPa)

4.3.2 Effect of parameter n' on specific moisture capacity B and volumetric strain ε_v

The effect of parameter n' on the variation in B is similar to the effect of parameter α. Figure 13 shows the variation in the specific moisture capacity due to the changes in suction for different n' values at the same value of α=1.0 (1/kPa). From the figure, it is seen that the value of B is smaller for higher values of suction. However, when the suction starts to decrease, the value of B increases and reaches a maximum peak that depends on the n' value; the greater parameter n', the greater the peak of B. After this peak, the value of B starts to decrease toward zero for P^C=0.

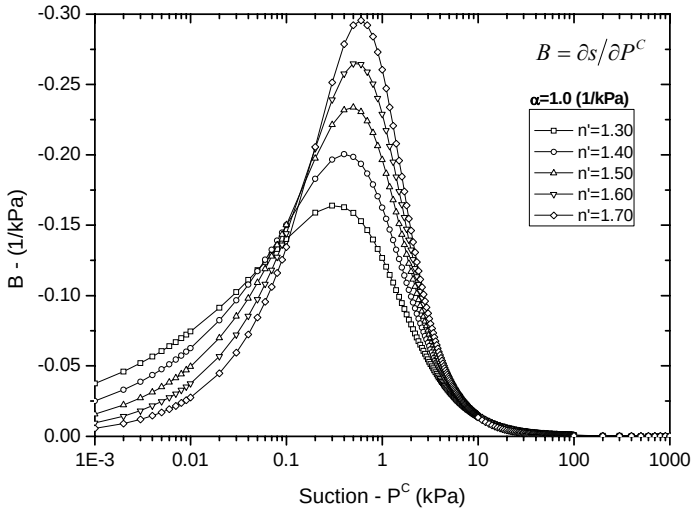

Figure 13: The influence of parameter n′ on the variation in B ($\partial s/\partial P^C$)

Figures 14 and 15 describe the influence of parameter n' on the development of volumetric strain ε_v in Element 12 in Figure 3 during the infiltration process for the two different cases, P^C_i=25.5 and 100 kPa, respectively. Five different values for parameter n' are used in order to observe their effect on the water infiltration process, namely, n'=1.2, 1.3, 1.4, 1.5, and 1.6, with α=1.0 (1/kPa). In the case of P^C_i=25.5 kPa (Figure 14), the volumetric strain is changing from positive volumetric strain (extension) at smaller values of n' to negative volumetric strain (contraction) at greater values of n'. The same trend is observed in the case of P^C_i=100 kPa (Figure 15). Similar to the effect of parameter α, the trend for greater contractive deformation is obtained for the greater n' values. An increase in parameter n' means an increase in B and the contractive behavior of the soil, thus, the potential for instability. This is consistent with the theoretical results obtained in the linear instability analysis in *Section 3*, where it was shown that the onset of instability increases when B increases and the volumetric strain is contractive. It can be said that, during the infiltration process, unsaturated materials with smaller n' values are less unstable than those with greater n' values.

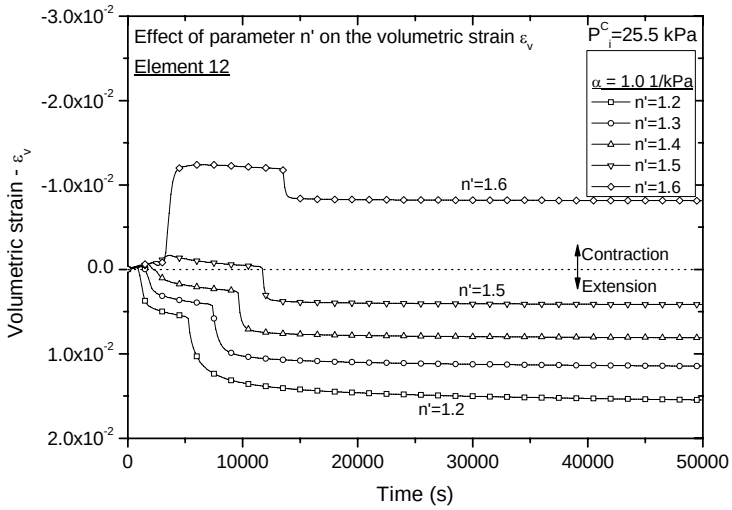

Figure 14: The Influence of parameter n' on the development of volumetric strain (P^C_i=25.5 kPa)

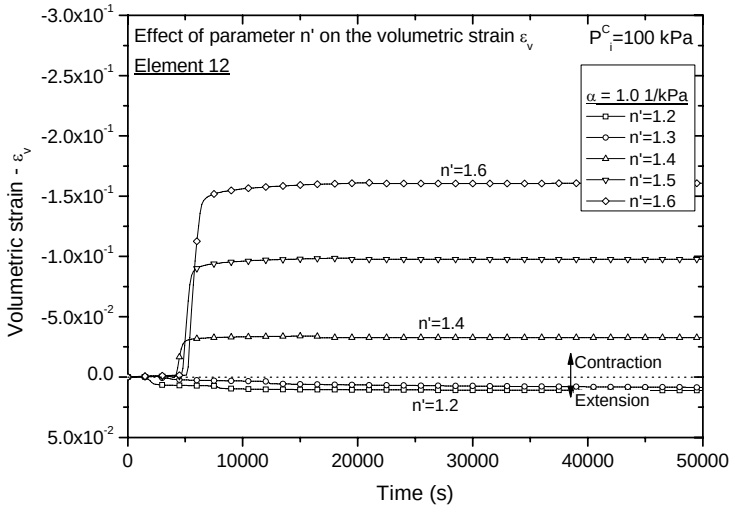

Figure 15: The influence of parameter n' on the development of volumetric strain (P^C_i=100 kPa)

4.4 Effect of initial suction P^C_i on volumetric strain ε_v

Suction is a main variable related to unsaturated soils. It has a direct effect on the stress variables, the soil water characteristic curve, the hydraulic conductivity, and the deformation characteristics. From the instability analysis presented in *Section 3*, it is seen

that suction P^C has an additional effect on the stability since it is included in A and B. The results of the instability analysis shown in Equation (83) suggest that a material with a greater initial suction $P^C{}_i$ is expected to contribute more to the onset of instability than a material with a smaller initial suction.

Figures 16 and 17 show the time histories of volumetric strain for two different parameters, α=1.0, 2.0 (1/kPa), respectively. On these graphs, a comparison is made for the two different levels of initial suction ($P^C{}_i$=25.5 and 100 kPa), while parameter n' is increased. From the figures, it is seen that the trend for greater contractive volumetric strain is obtained for the greater initial suction ($P^C{}_i$=100 kPa) when the same parameter n' is compared. This implies that the volumetric strain develops prominently during the wetting process when unsaturated materials present higher suctions. This is consistent with the theoretical results obtained in the instability analysis, namely, an increase in suction leads to an increase in the onset of the instability of the material system. It can be said that in a wetting process, the unsaturated materials with smaller suction values are less unstable than those with greater suction values.

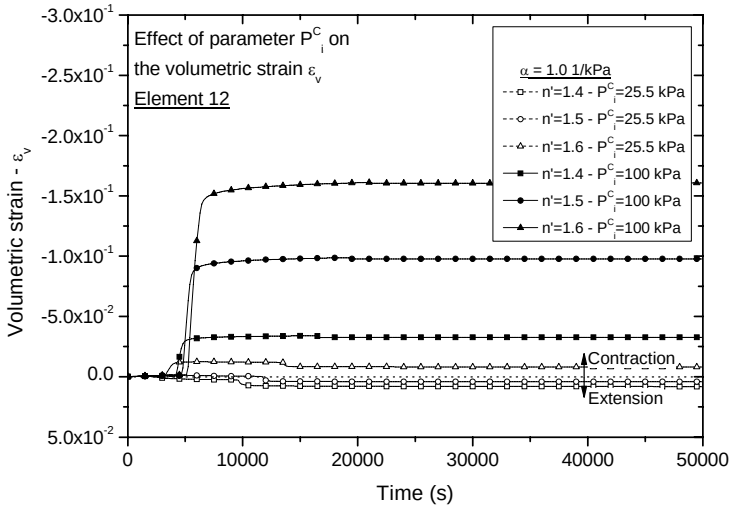

Figure 16: The influence of initial suction $P^C{}_i$ on the development of volumetric strain (α=1.0 1/kPa)

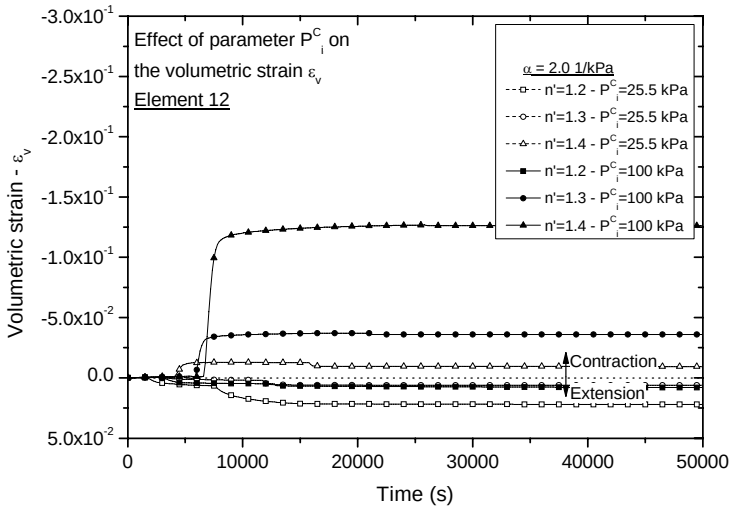

Figure 17: The influence of initial suction P^C_i on the development of volumetric strain (α=2.0 1/kPa)

4.5 Summary of the simulation results

Firstly, the results of the calculated settlements at the top of the soil-column and at the end of the infiltration process for different parameters α and n' and initial suction P^C_i=25.5 kPa are shown in Figure 18. Figure 18 indicates that for each parameter α, the initial behavior of the soil is expansive for the smaller n' values. When parameter n' is large, however, the behavior changes to be contractive (except for α=0.10 (1/kPa)). Two different types of instability are observed during the simulation process for the cases when P^C_i=25.5 kPa: a) for the cases when α=0.10 to 4.00 (1/kPa), the settlement increases with the increase in parameter n' until the peak where the settlement starts to decrease and changes to swelling. The rate of change from contractive to expansive behavior is larger for the larger α values. For n' values larger that those shown by the solid square (■) in Figure 18, the instability emerged due to an abrupt transition from the unsaturated to the saturated state presented at the very beginning of the calculation. In these cases, the instability is apparently triggered by the rapid saturation in the soil column due to the larger values of the specific moisture capacity (owing to the larger n' values) which leads to the generation of a large expansive deformation in the soil column.

The instability for the simulation with constant α=0.1 (1/kPa) was attained when n'=8.5. b) In the cases of greater parameters, namely, α=6.0, 8.0, and 10.0 (1/kPa), the instability occurred at the contractive side after the settlement reached a value between 0.15 and 0.20 m. From Figure 18, it is also possible to see that the rate of deformation increases when parameter α increases.

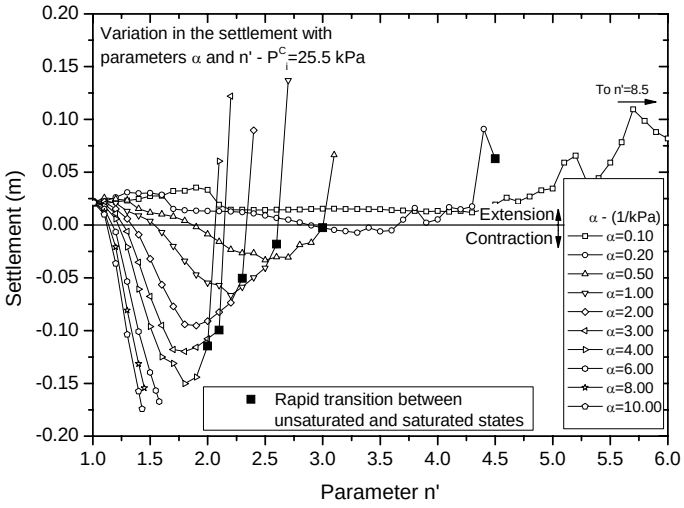

Figure 18: Variation in settlement with parameters α and n' (P^C_i=25.5 kPa)

Similarly, Figure 19 shows the calculated settlements for the case of the initial suction P^C_i=100 kPa; similar behavior to that observed in the case of initial suction P^C_i=25.5 kPa for the larger parameters α is shown. The instability is attained after the settlement reached values between 0.15 and 0.20 m, and the settlement increases with an increase in parameters α and n'. In this case, however, the deformation rates are larger and the instability always occurs at the contractive side. This suggests that soils with higher levels of suction are prone to be unstable due to the highly contractive behavior triggered by a wetting process. In this case, where the contractive behavior increases, both volumetric strain ε_v and strain rate $\dot{\varepsilon}$ are negative. As a result, and according to Equations (83) and (84), the potential for instability increases. The results in Figures 18 and 19 are consistent with the instability results obtained in *Section 3*, where it was found

that the onset of instability increases if the behavior of the material is contractive and both specific moisture capacity B and suction P^C increase.

In the simulations, the numerical instability is reached after a large contractive deformation is obtained. As a result, the numerical calculation abruptly ends due to the large increase in the deformation.

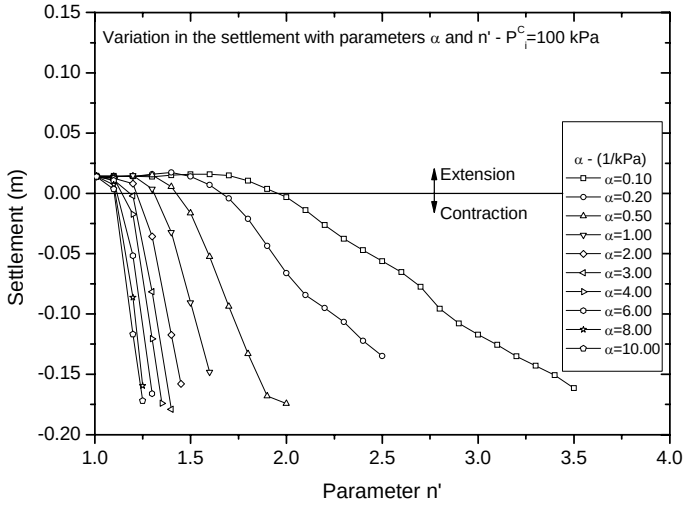

Figure 19: Variation in settlement with parameters α and n' (P^C_i=100 kPa)

The results of the simulations described in *Subsection 4.1* are summarized in a stability chart in order to observe the potentially stable region for the one-dimensional water infiltration problem. Figures 20 and 21 show the results of the simulation for different values of parameters α and n' and for the initial levels of suction P^C_i=25.5 and 100 kPa, respectively. In these figures, the solid circle (●) indicates the stable simulation results, while the **x** indicates the unstable simulation results (large increase in the volumetric deformation). On the graphs, the boundaries between the material-stable and -unstable regions (continuous line) and the boundary between expansive and contractive behaviors (dashed line) are shown. From Figures 20 and 21, the following characteristics can be understood:

1. The expansive behavior is presented for materials with smaller parameters α and n', but the contractive behavior is obtained when these parameters increase.

2. For the same parameter α, the potential for instability increases when parameter n' is large. A larger parameter n' leads to an increase in B and an increase in the deformation.
3. For the same parameter n', the instability potential increases when parameter α becomes large. This larger parameter α leads to an increase in B, and consequently, to an increase in the deformation.
4. It is possible to see that the material stable-unstable boundaries and the expansive-contractive boundaries shrink as the suction increases. It happens when P^C_i is changed from 25.5 kPa to 100 kPa.
5. The instability obtained by the numerical analyses is consistent with the theoretical results obtained by the linear instability analysis presented in *Section 3*.

According to the instability results, it can be said that unsaturated soils that are prone to instability during a wetting process are those with higher levels of initial suction, e.g., clays, as well as soils that are represented by a steeper soil water characteristic curve, e.g., sands.

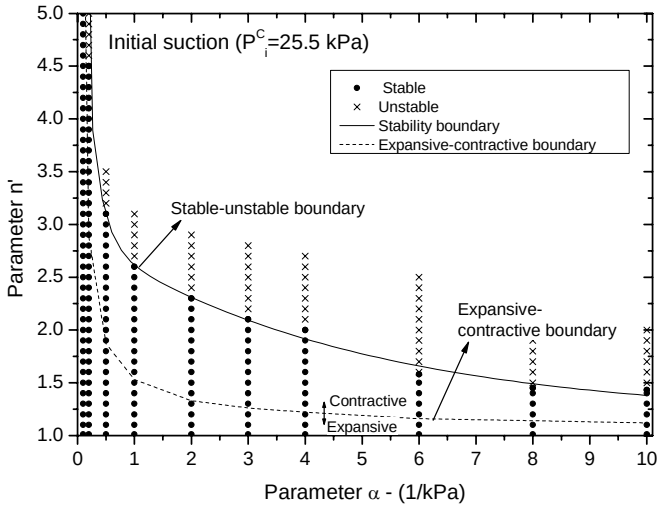

Figure 20: Stable and unstable regions for parameters α and n' during the infiltration process (P^C_i=25.5 kPa)

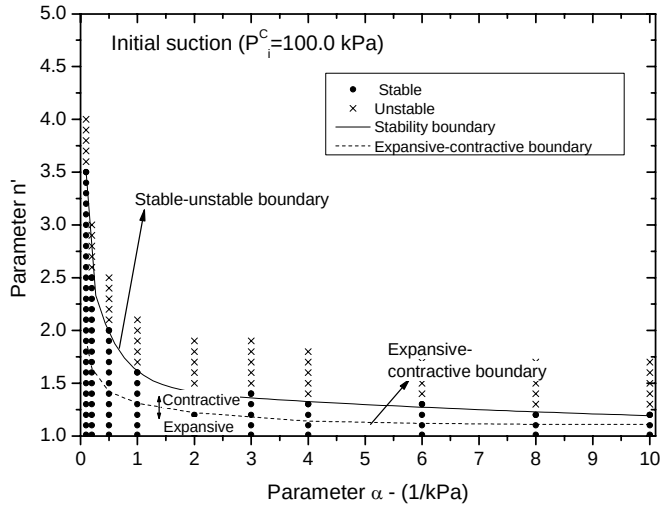

Figure 21: Stable and unstable regions for parameters α and n' during the infiltration process (P^C_i=100 kPa)

4.6 Stress paths and strain-time responses during wetting

In the simulation of the one-dimensional infiltration problem, the soil column is considered to be in its initial state with constant suction. The initial mean skeleton stress and the initial saturation are different, however, because different van Genuchten parameters (α and n') are used in each simulation. Now, in Figure 22, we will examine the effect of n' in detail by the stress paths ($\sqrt{2J_2}$ – σ'_m) for Element 12, for three values of parameter n', n'=1.4, 2.0, and 2.9, with the other parameters being held constant, namely, α=1.0 1/kPa and P^C_i=25.5 kPa. The cases of n'=1.4 and 2.0 correspond to the stable region, while the case of n'=2.9 is on the unstable region, in Figure 20. In the case of n'=1.4, it is seen that the stress path follows a direction toward the critical state line (A-A'-A"), whereas for n'=2.0, the stress path initially goes in the opposite direction during the unsaturated state (B-B') and then returns toward the critical state line in the saturated state (B'-B"). When n'=2.9, it is seen that the stress path approaches the critical state line and reaches the state with almost zero deviator stress. After that, the path goes to C" (C-C'-C").

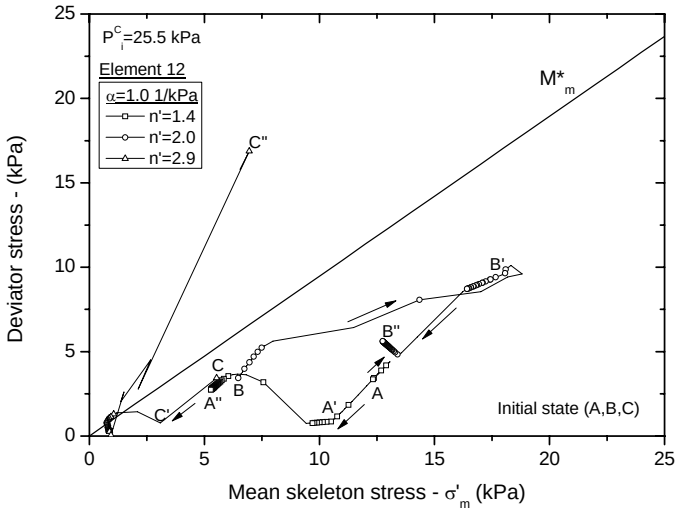

Figure 22: Stress path during the wetting process - $\sqrt{2J_2}-\sigma'_m$ space (P^C_i=25.5 kPa)

The saturation-mean skeleton stress relations, which correspond to Figure 22, are presented in Figure 23. This figure shows that the larger the parameter *n'*, the smaller the initial saturation, namely, points A, B, and C. The initial saturation significantly affects the initial mean skeleton stress because the mean skeleton stress depends on the saturation that is included in the calculation of the average pore pressure, as shown in Equations (11) and (12). For the same suction, the larger the saturation, the smaller the average pore pressure; hence, the initial mean skeleton stress is large. Figure 23 also shows that for the case of *n'*=2.9, once full saturation has been attained, the mean skeleton stress decreases and then increases (C'-C"). Figure 24 illustrates the suction-mean skeleton stress relations. As shown in Figure 24, for the same initial suction, the values for the initial mean skeleton stress are different at points A, B, and C. The larger the value of *n'*, the smaller the initial mean skeleton stress. During the infiltration process, when the water reaches the element, the suction starts to decrease and the mean skeleton stress decreases or increases depending on the value of *n'*. For *n'*=1.4, the mean skeleton shows a small decrease in the unsaturated state (A-A'), while for *n'*=2.0, the mean skeleton stress increases (B-B'). In the case of *n'*=2.9, the mean skeleton stress reduces with the reduction in suction and then finally increases (C-C'-C").

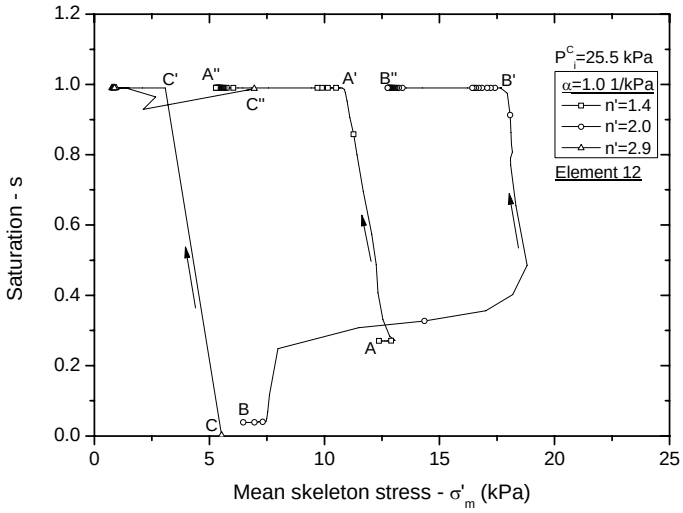

Figure 23: Saturation–mean skeleton stress relation – s-σ'_m (P^C_i=25.5 kPa)

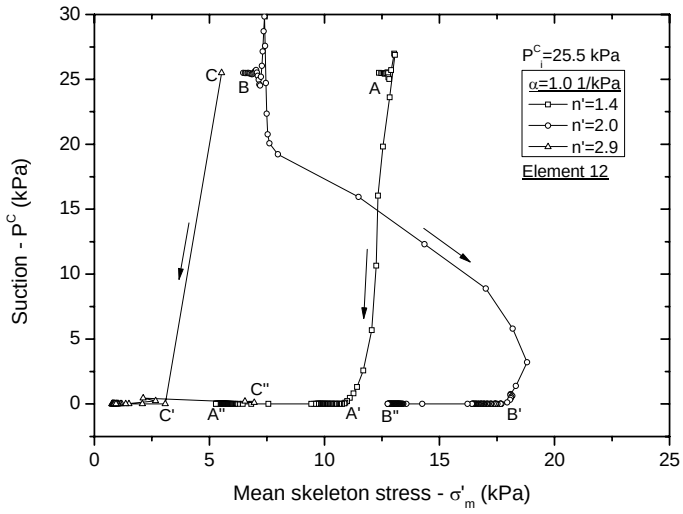

Figure 24: Suction–mean skeleton stress relation – P^C-σ'_m (P^C_i=25.5 kPa)

The accumulated viscoplastic shear strain (γ^{vp})–time histories are shown in Figure 25. It is observed that the development of irrecoverable deformation is very small for the parameter n'=1.4. For the larger value of n'=2.0, however, the accumulated viscoplastic shear strain develops prominently during the transition of the material from the unsaturated state to the saturated state up to γ^{vp}=10.3%. For the case of n'=2.9, the

accumulated viscoplastic shear strain develops from the beginning of the process until it reaches a value of 3%, and it remains almost constant before suddenly increasing. This indicates that large irrecoverable deformation has developed in the soil column. Similarly, the time histories of the volumetric strain are shown in Figures 26. The development of the volumetric deformation in time indicates that different responses of the column are obtained during the wetting process for different parameters n'. For n'=1.4, the volume increases slightly due to the decrease in mean skeleton stress, mainly because of the increase in pore water pressure. For n'=2.0, however, the volume decreases due to the increase in mean skeleton stress, mainly because of the increase in the total stress. In the case of n'=2.9, it is seen that the volume increases at the beginning of the process, and it remains constant for some time before an abrupt change to large contraction. The increase in volumetric strain at the beginning of the simulation can be explained by the rapid saturation of the soil owing to a steeper soil water characteristic curve represented by the larger parameter n'. This significant transition also leads to the diminution of the mean skeleton stress with suction, namely, C-C' in Figure 24.

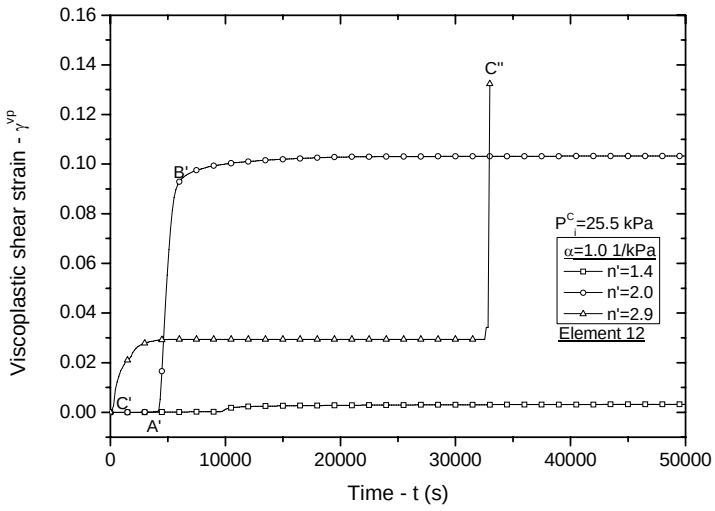

Figure 25: Time history of viscoplastic shear strain (P^C_i=25.5 kPa)

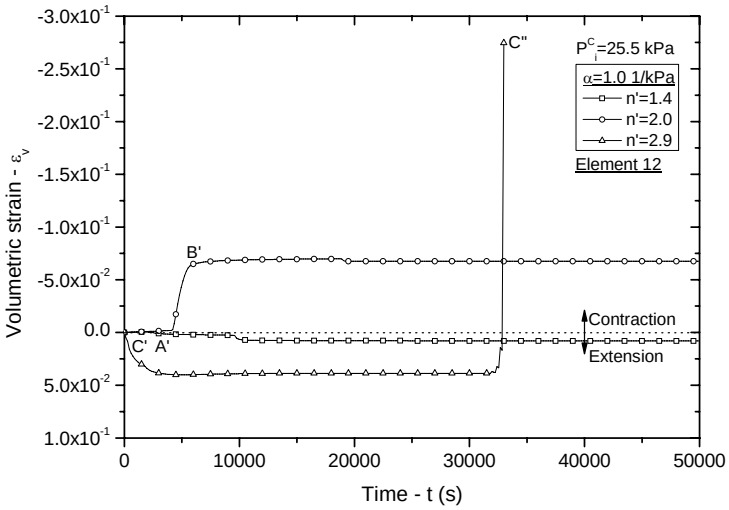

Figure 26: Time history of volumetric strain ($P^C{}_i$=25.5 kPa)

From the above discussion using Figures 22-26, it is seen that a larger value of n', i.e., a steeper suction-saturation characteristic curve, leads to the development of larger strain. This result is consistent with the instability analysis presented in Section 3. In addition, it is worth noting that contractive volumetric strain occurs when large strain develops, namely, for the case of relatively unstable behavior (Barden et al., 1973; Lloret and Alonso, 1980; Wheeler and Sivakumar, 1995).

5. CONCLUSIONS

In order to study the effects of parameters and state variables on the instability of an unsaturated material system during a wetting process, a theoretical analysis was conducted with a simplified viscoplastic model. It was found that in both hardening and softening ranges, the occurrence of the instability of an unsaturated material system is more likely (the rate of the fluctuation grows) if suction P^C and specific moisture capacity $B=\partial s/\partial P^C$ are larger. Moreover, the onset of instability can be increased if the strain rate is negative ($\dot{\varepsilon} < 0$), and the behavior of the material is contractive ($\varepsilon_v < 0$), while the slope of curve $\sigma'_{mb} - P^C$ ($A=\partial \sigma'_{mb}/\partial P^C$) increases. It was also found that the effect of the

specific moisture capacity and the suction is more significant than the effect of the slope of curve σ'_{mb}-P^C.

From the numerical study on the one-dimensional infiltration problem, it was found that the elasto-viscoplastic material system is more unstable when parameters α and n' are large, namely, for large values of the slope of the soil water characteristic curve (specific moisture capacity). For the effect of the suction, it is observed that the instability significantly increased when the initial suction of the unsaturated material was increased (P^C_i=25.5 to 100 kPa). These trends are consistent with the theoretical results obtained by the linear instability analysis.

The simulated settlements show that for smaller parameters α and n', the material behavior is expansive. Nevertheless, when these parameters become large, the expansive behavior of the soils changed to a contractive one. Parameters α and n' indicate a great effect on the development of the deformation. The greater the parameters α and n', the larger the settlements obtained. Larger rates of settlement were also obtained for higher levels of initial suction. This suggests that rapid transitions from unsaturated to saturated states and higher levels of suction lead to contractive behavior and instability; e.g., a wetting-induced collapse.

REFERENCES

Alonso, E.E., Gens, A., Delahaye, C.H., 2003. Influence of rainfall on the deformation and stability of a slope in overconsolidated clays: a case study. Hydrogeol. J. 11, 174-192.

Alonso, E.E., Gens, A., Josa, A., 1990. A constitutive model for partially saturated soils. Géotechnique 40(3), 405-430.

Atkin, R.J., Craine, R.E., 1976. Continuum theories of mixtures: basic theory and historical developments. Q. J. Mech. Appl. Math. 29(2), 209-244.

Barden, L., McGown, A., Collins, K., 1973. The collapse mechanism in partly saturated soil. Eng. Geol. 7, 49-60.

Biot, M.A., 1962. Mechanics of deformation and acoustic propagation in porous media. J. Appl. Phys. 33(4), 1482-1498.

Bowen, R.M., 1976. Theory of mixtures, in: Eringen, A.C. (Ed), Continuum Physics, Vol. III, Academic Press, New York, pp. 1-127.

Buscarnera, G., Nova, R., 2009a. Modelling the onset of instability in oedometric tests on unsaturated bounded soils. In: Pietruszczak, S., Pande, G.N., Tamagnini, C., Wan, R. (Eds.), Computational Geomechanics, ComGeo I, First International Symposium on Computational Geomechanics, Juan-les-Pins, France, pp. 226-238.

Buscarnera, G., Nova, R., 2009b. Modelling instabilities in triaxial testing on unsaturated soil specimens. Int. J. Numer. Anal. Methods Geomech. doi: 10.1002/nag.832.

Cho, S.E., Lee, S.R., 2001. Instability of unsaturated soil slopes due to infiltration. Comput. Geotech. 28, 185-208.

Cui, Y.J., Delage, P., 1996. Yielding and plastic behaviour of an unsaturated compacted silt. Géotechnique 46(2), 291-311.

Cunningham, M.R., Ridley, A.M., Dineen, K., Burland, J.B., 2003. The mechanical behaviour of a reconstituted unsaturated silty clay. Géotechnique 53(2), 183-194.

Ehlers, W., Graf, T., Ammann, M., 2004. Deformation and localization analysis of partially saturated soil. Comput. Methods Appl. Mech. Eng. 193, 2885-2910.

Ehlers, W., Volk, W., 1998. On theoretical and numerical methods in the theory of porous media based on polar and non-polar elasto-plastic solid materials. Int. J. Solids Struct. 35(34,35), 4597-4617.

Feng, H., 2007. Multiphase deformation analysis of elasto-viscoplastic unsaturated soil and modeling of bentonite, PhD thesis, Kyoto University, Japan.

Fung, Y.C., Tong, P., 2001. Plasticity: Classical and Computational Solid Mechanics. World Scientific, Singapore.

Garcia, E., Oka, F., Kimoto, S., 2010. Numerical analysis of a one-dimensional infiltration problem in unsaturated soil by a seepage-deformation coupled method. Int. J. Numer. Anal. Methods Geomech. doi: 10.1002/nag.908.

Higo, Y., Oka, F., Jiang, M., Fujita, Y., 2005. Effects of transport of pore water and material heterogeneity on strain localization of fluid-saturated gradient-dependent viscoplastic geomaterial. Int. J. Numer. Anal. Methods Geomech. 29, 495-523.

Higo, Y., Oka, F., Kodaka, T., Kimoto, S., 2006. Three-dimensional strain localization of water-saturated clay and numerical simulation using an elasto-viscoplastic model. Philos. Mag. 86(21), 3205-3240.

Jennings, J.E.B., Burland, J.B., 1962. Limitations to the use of effective stresses in partly saturated soils. Géotechnique 12, 125-144.

Kato, R., Sunami, S., Oka, F., Kimoto, S., Kodaka, T., 2009. A seepage-deformation coupled analysis method for unsaturated river embankments. In: Oka, F., Murakami, A., Kimoto, S. (Eds.), Proceedings of the International Symposium on Prediction and Simulation Methods for Geohazard Mitigation (IS-KYOTO2009), Kyoto, Japan, Taylor & Francis Group, London, UK, pp. 401-407.

Khalili, N., Geiser, F., Blight, G.E., 2004. Effective stress in unsaturated soils: Review with new evidence. Int. J. Geomech. 4(2), 115-126.

Kimoto, S., Oka, F., 2005. An elasto-viscoplastic model for clay considering destructuralization and consolidation analysis of unstable behavior. Soils Found. 45(2), 29-42.

Kimoto, S., Oka, F., Fushita, T., 2010. A chemo-thermo-mechanically coupled analysis of ground deformation induced by gas hydrate dissociation. Int. J. Mech. Sci. 52(2), 365-376.

Kimoto, S., Oka, F., Fushita, T., Fujiwaki, M., 2007. A chemo-thermo-mechanically coupled numerical simulation of the subsurface ground deformations due to methane hydrate dissociation. Comput. Geotech. 34, 216-228.

Kimoto, S., Oka, F., Higo, Y., 2004. Strain localization analysis of elasto-viscoplastic soil considering structural degradation. Comput. Methods Appl. Mech. Eng. 193, 2845-2866.

Lloret, A., Alonso, E.E, 1980. Consolidation of unsaturated soils including swelling and collapse behaviour. Géotechnique 30(4), 449-477.

Loret, B., Prévost, J.H., 1991. Dynamic strain localization in fluid-saturated porous media. J. Eng. Mech. 117, 907-922.

Lu, N., Likos, W.J, 2004. Unsaturated Soil Mechanics. Wiley, New Jersey.

Nemat-Nasser, S., 2004. Plasticity: A Treatise on Finite Deformation of Heterogeneous Inelastic Materials. Cambridge University Press, Cambridge.

Oka, F., Adachi, T., Yashima, A., 1994. Instability of an elasto-viscoplastic constitutive model for clay and strain localization. Mech. Mater. 18, 119-129.

Oka, F., Adachi, T., Yashima, A., 1995. A strain localization analysis using a viscoplastic softening model for clay. Int. J. Plasticity 11(5), 523-545.

Oka, F., Kimoto, S., Takada, N., Higo, Y., 2009. A multiphase elasto-viscoplastic analysis of an unsaturated river embankment associated with seepage flow. In: Oka, F., Murakami, A., Kimoto, S. (Eds.), Proceedings of the International Symposium on Prediction and Simulation Methods for Geohazard Mitigation (IS-KYOTO2009), Kyoto, Japan, Taylor & Francis Group, London, UK, pp. 127-132.

Oka, F., Kodaka, T., Kim, Y.S., 2004. A cyclic viscoelastic-viscoplastic constitutive model for clay and liquefaction analysis of multi-layered ground. Int. J. Numer. Anal. Methods Geomech. 28, 131-179.

Oka, F., Kodaka, T., Kimoto, S., Kim, Y.S., Yamasaki, N., 2006. An elasto-viscoplastic model and multiphase coupled FE analysis for unsaturated soil. In: Miller, G.A., Zapata, C.E., Houston, S.L., Fredlund, D.G. (Eds.), Fourth international conference on unsaturated soils, Geotechnical Special Publication, ASCE, Carefree, Arizona, 147(2), 2039-2050.

Oka, F., Kodaka, T., Suzuki, H., Kim, Y.S., Nishimatsu, N., Kimoto, S., 2010. Experimental study on the behavior of unsaturated compacted silt under triaxial compression. Soils Found. 50(1), 27-44.

Pinder, G.F., Gray, W.G, 2008. Essentials of Multiphase Flow and Transport in Porous Media. Wiley, Hoboken, New Jersey.

Rice, J.R., 1975. On the stability of dilatant hardening for saturated rock masses. J. Geophys. Res. 80(11), 1531-1536.

Schrefler, B.A., Majorana, C.E., Sanavia, L., 1995. Shear band localization in saturated porous media. Arch. Mech. 47(3), 577-599.

Sheng, D., Sloan, S.W., Gens, A., Smith, D.W., 2003. Finite element formulation and algorithms for unsaturated soils. Part I: Theory. Int. J. Numer. Anal. Methods in Geomech. 27(9), 745-765.

Terzaghi, K., 1943. Theoretical Soil Mechanics. Wiley, New York.

Thomas, H.R., He, Y., 1998. Modelling the behaviour of unsaturated soil using an elastoplastic constitutive model. Géotechnique 48(5), 589-603.

Van Genuchten, M.T., 1980. A closed-form equation for predicting the hydraulic conductivity of unsaturated soils. Soil Sci. Soc. Am. J. 44, 892-898.

Wheeler, S.J., Karube, D., 1996. State of the art report: Constitutive modelling. In: Alonso, E.E., Delage, P. (Eds.), Proceedings of the First International Conference on Unsaturated Soils, Paris, France, Balkema, Rotterdam, The Netherlands, pp. 1323-1356.

Wheeler, S.J., Sivakumar, V., 1995. An elasto-plastic critical state framework for unsaturated soil. Géotechnique 45(1), 35-53.

Wu, L.Z., Zhang, L.M., 2009. Analytical solution to 1D coupled water infiltration and deformation in unsaturated soils. Int. J. Numer. Anal. Methods Geomech. 33, 773-790.

Table captions

Figure captions